

An Experimental Evaluation of a 3D Visible Light Positioning System in an Industrial Environment with Receiver Tilt and Multipath Reflections

Yousef Almadani^{1*}, Muhammad Ijaz¹, Bamidele Adebisi¹, Sujan Rajbhandari², Sander Bastiaens³, Wout Josphe³, and David Pleys³

¹*Manchester Metropolitan University, Faculty of Science and Engineering, Department of Engineering, Manchester, M1 5GD, United Kingdom*

²*Huawei Technologies Sweden AB, 41250 Gothenburg, Sweden*

³*Ghent University, imec-WAVES, Department of Information Technology, iGent-Technologiepark 126, Ghent, 9052, Belgium*

Abstract

In this paper, two different three-dimensional (3D) indoor visible light positioning (VLP) algorithms are experimentally assessed for an industrial environment. The Cayley-Menger determinant (CMD) and linear least square (LLS) trilateration algorithms use the received signal strength (RSS) to estimate the receiver's 3D position without prior knowledge of its height. The unknown 3D position of the receiver is estimated by the trilateration algorithms coupled with a cost function under different realistic scenarios. The performances of the algorithms are experimentally evaluated in terms of positioning error by considering two different light-emitting diode (LED) configurations in the presence of different receiver tilt angles, and with multipath reflections. It is observed that the widespread square LED configuration results in position ambiguities while a star-shaped configuration is much more accurate. Experimental tests performed in a 4 m × 4 m × 4.1 m area with four LEDs reported a median positioning error of 10.6 and 10.5 cm using the LLS and CMD algorithms, respectively, without the presence of receiver tilt or multipath reflections. However, when a receiver tilt of 10° was added, the median error increased to 22.7 cm using the LLS algorithm and 21.6 cm using the CMD algorithm. Overall, the achieved mean and maximum values using the LLS algorithm were 13.1 and 39 cm, respectively, while they were 12.2 and 34 cm using the CMD algorithm.

Key words: indoor visible light positioning, localization, industrial, tilt, VLC, VLP

1. Introduction

Indoor positioning is a very promising research domain that is gaining wide attention due to its potential in Industry 4.0 and the health sector. Conventional positioning methods that rely on satellites such as global positioning system (GPS) are unreliable for indoor positioning due to the high penetration loss from walls and building materials. Complementary methods such as assisted-GPS and pseudo-satellite have been proposed to address the shortcomings of conventional satellite-based systems. However, the accuracies of these systems are still inadequate with the added complexity of integrating two different systems [1]. Other technologies have also been proposed for indoor positioning and navigation such as Bluetooth, ultrasound, ultra-wideband (UWB), and radio-frequency (RF) based techniques [2]. While encouraging results have been achieved using Bluetooth and UWB, there is also another emerging technology that makes use of the ubiquitous light fixture's infrastructure.

Visible light positioning (VLP) is one of the most promising technologies being proposed for indoor positioning given the readily available lighting infrastructure and its many advantages such as increased bandwidth, security and low relative complexity when compared with RF-based positioning. While most of the technologies being researched and proposed for indoor localization are based on the highly congested RF spectrum, VLP systems are not sensitive to electromagnetic interference, which enables them to be used in areas that are sensitive to electromagnetic waves such as hospitals and certain power plants [3].

2. Related Work

In [4], the researchers proposed a multiple-classifiers fusion localization framework by using received signal strength (RSS) fingerprints. The experiment was performed within a $0.7 \text{ m} \times 0.7 \text{ m}$ area with four LEDs and achieved a median square positioning error of less than 5 cm for the majority of the area. In [5], a 3D VLC positioning system based on modified particle swarm optimization (PSO) algorithm is presented and has been experimentally tested. The researchers evaluated the system using four LEDs in a cube

33 frame measuring $0.9 \text{ m} \times 0.9 \text{ m} \times 1.5 \text{ m}$ and achieved an average error of
 34 3.5 cm for a 3D VLP system. In [6], a machine learning (ML) technique with
 35 height tolerance was tested using three LEDs within an area of $1.1 \text{ m} \times 1 \text{ m}$
 36 $\times 2.5 \text{ m}$. The result shows that over 80% of the results can be under 5 cm
 37 with an improved height tolerance range of 15 cm . Researchers in [7] intro-
 38 duced and experimentally tested a VLP method based on median shift (MS)
 39 algorithm and unscented Kalman filter (UKF) using image sensors. The test
 40 area of their experimental setup was $1.9 \text{ m} \times 1 \text{ m} \times 1.9 \text{ m}$ and achieved a
 41 positioning accuracy of up to 0.42 cm , with an accuracy of 1.41 cm when half
 42 of the LED was shielded. The work in [8] used an RSS-based VLP system
 43 combined with a deep neural network based on the Bayesian Regularization
 44 (BR-DNN) with a sparse diagonal training data set. The method was tested
 45 in a $1.8 \text{ m} \times 1.8 \text{ m} \times 2.1 \text{ m}$ area and achieved a maximum positioning error
 46 of 4.58 cm for an even set, and 3.4 cm under a diagonal set of LEDs. In
 47 [9], a low-complexity time-difference-of-arrival (TDoA) method with an en-
 48 hanced practical localization using cross-correlation is reported and achieved
 49 a positioning accuracy of 9.2 cm in a $1.2 \text{ m} \times 1.2 \text{ m}$ testbed area. A 2D
 50 VLP system using differential phase difference of arrival (DPDoA) was ex-
 51 perimentally tested in [10] and achieved an average root-mean-square (RMS)
 52 positioning error of 1.8 cm and a maximum of 8 cm in a testbed area of
 53 $1 \text{ m} \times 1.2 \text{ m} \times 2 \text{ m}$. Researchers in [11] proposed a fusion positioning
 54 system based on extended Kalman filters (EKF), which uses an inertial nav-
 55 igation unit to improve the performance of the VLP system. An average
 56 positioning error of 33.9 cm was achieved based on RSS alone and 14.5 cm
 57 when combined with an EKF.

58 Three typical office environments were tested in [12]. Their proposed
 59 method locates the receiver using trilateration/multi-lateration if over three
 60 light sources are perceived, along with an optimization process. If less than
 61 three signals are received, then a fusion method is used with an inertial mea-
 62 surement unit (IMU). The achieved 90th percentile positioning errors for the
 63 three environments were 0.4 m , 0.7 m , and 0.8 m . When only one transmitter
 64 is available, the 90th percentile error increased to 1.1 m . The work in [13]
 65 proposed the use of the received light intensity with accelerometer measure-
 66 ments to compute distances between the transmitters and the receiver. An
 67 error of less than 25 cm was reported in a $5 \text{ m} \times 3 \text{ m} \times 3 \text{ m}$ area. A gain
 68 difference positioning method based on the angle of arrival and the received
 69 signal strength was proposed in [14]. The method uses multiple tilted re-
 70 ceivers to calculate the 3D location with reported average error distances of

Table 1: A summary of the experimental work in indoor VLP systems

Ref.	Method	2D/3D	Test Area (W L H) (m)	Accuracy (cm)	No. of LEDs
[4]	Fingerprints	2D	$0.7 \times 0.7 \times 1.48$	5	4
[6]	RSS w/ ML	3D	$1.1 \times 1 \times 2.5$	3.65	3
[7]	MS-UKF	2D	$1.9 \times 1 \times 1.9$	0.42	4
[8]	RSS w/ BR-DNN	2D	$1.8 \times 1.8 \times 2.1$	4.58	4
[9]	TDoA	2D	$1.2 \times 1.2 \times 2$	9.2	3
[10]	DPDoA	2D	$1 \times 1.2 \times 2$	1.8	3
[11]	RSS	2D	$2.5 \times 2.84 \times 2.5$	33.9	7
	RSS-EKF	2D		14.5	
[13]	RSS w/ Accelerometer	3D	$5 \times 3 \times 3$	25	3
[14]	RSS ratio	3D	$2 \times 2 \times 2.5$	3	1 w/ multiple PDs
[5]	PSO	3D	$0.9 \times 0.9 \times 1.5$	3.492	4
[15]	LED-ID w/ ROS	2D	$1 \times 1 \times 1.5$	0.82	4
[16]	LED-ID w/ ROS & ML	2D	$0.8 \times 0.8 \times 2$	2	5
			5×8	45	
[12]	RSS w/ IMU	3D	2×12	70	5
			3.5×6.5	80	

71 less than 3 cm. Table 1 provides a summary of the discussed experimental
72 work on indoor VLP systems.

73 In [15], the researchers proposed an indoor robot VLP positioning package
74 based on robot positioning system (ROS) with a efficient LED-ID detection
75 scheme for rolling shutter. The system was experimentally tested in a 1 m
76 \times 1 m \times 1.5 m area with 36 uniformly distributed test points. The results
77 reported an average accuracy of 0.82 cm, while 90% of the errors were less
78 than 1.417 cm. The work in [16] proposed a double light positioning algo-
79 rithm. The system uses LED-ID to determine the position of a receiver as
80 well as a CMOS image sensor combined with machine learning a algorithm
81 to identify the LED-ID. The system was tested in a 0.8 m \times 0.8 m \times 2 m
82 area and all of the reported positioning errors were within 3.85 cm with an
83 average accuracy of 2 cm

84 As can be seen, the majority of the experimental work studied the perfor-
85 mance of 2D VLP systems and generally required the use of additional hard-
86 ware or the use of some complex algorithm for 3D localization. Additionally,
87 most of the experiments analyzed the performance in relatively very small
88 areas. In contrast to some of the previous works by other researchers, this
89 paper examines a purely RSS-based 3D VLP system in a higher and larger
90 area without the need for an additional receiver or complex algorithms.

91 In this paper, we experimentally assess and compare the performances
92 of two 3D VLP positioning algorithms under different scenarios that are
93 realistic industrial environments. The Cayley-Menger determinant (CMD)

94 and linear least square (LLS) algorithms are coupled with a cost function
 95 to estimate a true 3D position without prior knowledge of the receiver's
 96 height. The algorithms are evaluated for two different LED configurations
 97 with different degrees of receiver tilt, and in the presence of a filled storage
 98 rack to examine the effect of multipath reflections on the performance. The
 99 algorithm could be used for VLP-based unmanned aerial vehicles (UAVs)
 100 tracking in industrial warehouses. This is an emerging area where UAVs,
 101 or drones, are employed for different sets of application such as stock-taking
 102 in warehouses and inspecting hard-to-reach areas [17]. The commonly used
 103 RF-based technologies generally suffer from electromagnetic interference or
 104 unstable RF signals, deeming it unsuitable in providing high positioning
 105 accuracy. It is especially not suitable in environments that have constant
 106 sudden changes, e.g. forklifts or automated guided vehicles (AGVs), and
 107 movement of people. This paper is partly an extension of our previous work
 108 in [17]. However, this work considers an additional LED layout configuration,
 109 an additional receiver tilt angle value, considers the presence of storage rack,
 110 and examines the performance for 2D positioning as well.

111 The remainder of the paper is organized as follows: Section 3 details the
 112 experimental setup. Section 4 presents the system model and the positioning
 113 algorithms along with the cost function. Experimental results are presented
 114 in Section 5 and is then followed by a discussion of the main findings in
 115 Section 6. Finally, the paper concludes in Section 7.

116 3. Experimental Setup

117 The 3D algorithm is analyzed experimentally in a VLP lab that mea-
 118 sures $4\text{ m} \times 4\text{ m}$ with the height of the LEDs at approximately 4.1 m, as
 119 shown in Figure 1 (a). Black curtains are used as a substitute for walls
 120 to ensure that uncontrolled reflections from walls and objects are avoided.
 121 Four BXRE-50C3001-D-24 LEDs, shown in the inset of Figure 1 (a), are
 122 intensity-modulated using transmitting pulse trains with a duty cycle of 0.5
 123 with frequencies of 500 Hz, 1 kHz, 2 kHz, and 4 kHz. This ensures that the
 124 contributions from the different LEDs can be demultiplexed individually at
 125 the receiver's side.

126 The receiver is a commercial photodiode with an integrated electrical
 127 amplifier (PDA36A2¹ by Thorlabs) that has an active area A_{pd} of 13 mm^2 .

¹<https://www.thorlabs.com/thorproduct.cfm?partnumber=PDA36A2>

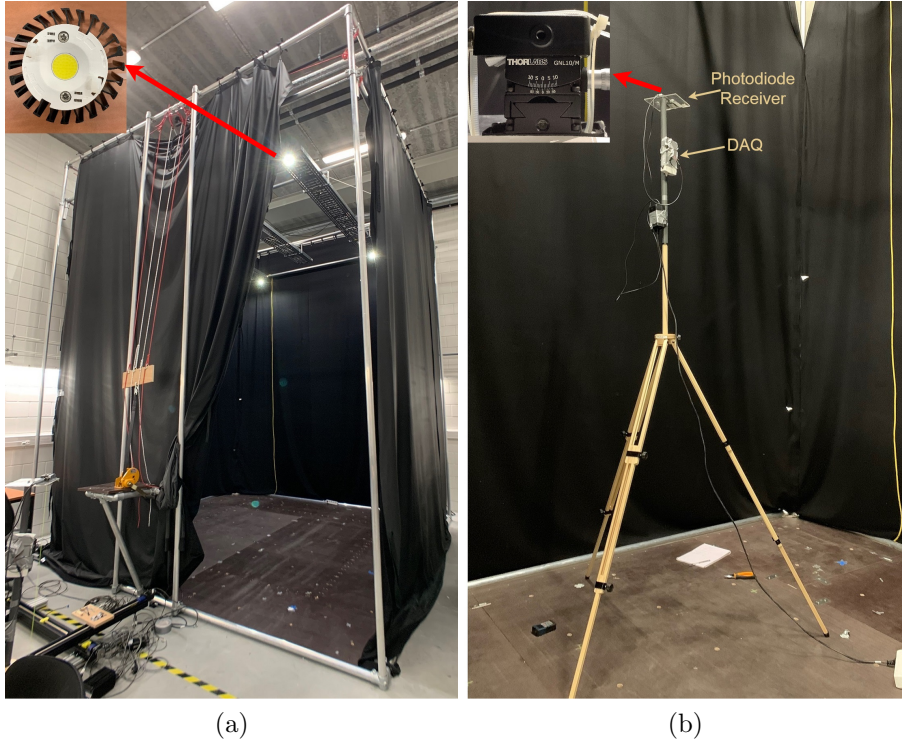


Figure 1: (a) The VLP lab experimental setup with black curtains with a view of the LEDs attached to ceiling rails, and (b) a tripod with the receiver mounted on top.

128 The photodiode’s responsivity was estimated at 0.22 A/W by weighing the
 129 photodiode’s responsivity spectrum with the LED’s spectrum. The receiver
 130 is attached to a tripod with a vertical pole that allows adjustment of the re-
 131 ceiver’s height as shown in Figure 1 (b). The data is acquired using National
 132 Instrument’s USB-6212 for processing. A fast Fourier transform (FFT)-based
 133 demodulation is used to extract the received power values for each LED in
 134 MATLAB[®], as specified in [18]. Table 2 shows the main parameters used in
 135 the experimental setup.

136 Figure 2 shows a path consisting of forty-eight points selected to take the
 137 receiver around the room at different heights ranging from 0.64 m to 2.55 m.
 138 The black line indicates the travel path, the green square denotes the start
 139 point, and red denotes the endpoint. The measurements were configured to
 140 sample 256 times using the DAQ with a sampling rate of 128 kHz. Twenty-

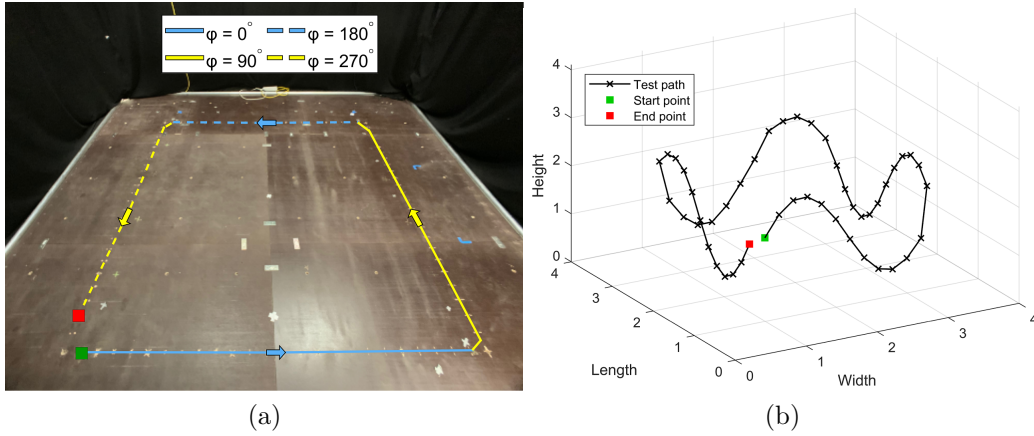


Figure 2: (a) The test path shown inside the VLP lab demonstrating the azimuthal orientation φ of the receiver; (b) A 3D view of the path demonstrating the height variations of the receiver along the specified path.

141 five power value readings were averaged at each location to reduce the impact
 142 of noise.

143 Two LED configurations denoted as ‘Square’ and ‘Star’ are used for the
 144 evaluation of the VLP as shown in Figure 3. The square-shaped is a typical
 145 configuration that is adopted by many researchers while the star configura-
 146 tion has a central LED circularly surrounded by the other three LEDs. Our
 147 previous work in [19] indicates that a classic configuration with four LEDs
 148 mounted in a square-shape is not able to accurately solve the 3D position
 149 ambiguity. Therefore, to counter this problem, a star-shaped configuration
 150 was proposed.

151 4. System Model

152 In this section, the VLC’s system model is outlined and the positioning
 153 algorithms along with the cost function are explained.

154 4.1. VLC System Model

155 The radiation of an LED chip follows a Lambertian pattern. Considering
 156 the line-of-sight (LoS) path between the LED transmitters and the receiver,

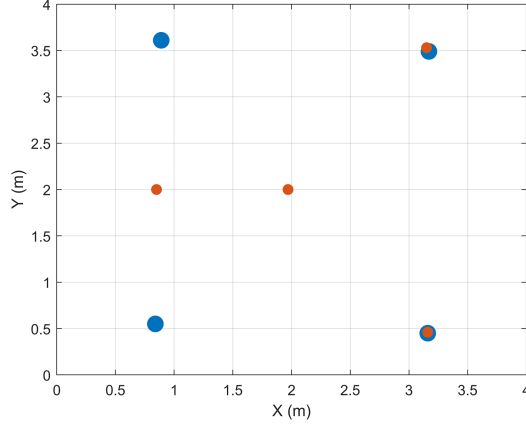


Figure 3: Top view of LEDs' locations in the with the blue dots representing the 'Square' configuration and the red dots representing the 'Star' configuration.

157 the received power can be modeled as [20]:

$$P_{ri} = P_{ti} \frac{(m+1)A_{pd}}{2\pi d_i^2} \cos^m(\alpha) \cos(\beta) T_{pd}(\beta) G_{pd}(\beta) \quad (1)$$

158 where P_{ti} is the transmitted power from the i^{th} LED, m is the Lambertian
 159 order, d_i is the distance between the i^{th} LED transmitter and the receiver,
 160 α is the angle of irradiance, β is the angle of incidence. The parameters are
 161 illustrated in Figure 4 (a). The optical filter's gain $T_{pd}(\beta)$, and the optical
 162 concentrator's gain $G_{pd}(\beta)$ are assumed to be equal to 1. Additionally, by
 163 assuming that the transmitters and the receiver are horizontally parallel,
 164 $\cos(\alpha) = \cos(\beta) = \frac{h_{LED}-z}{d_i} = \frac{\Delta h}{d_i}$, then d_i can be estimated as \hat{d}_i using the
 165 received signal power, P_{ri} [21]:

$$\hat{d}_i = \sqrt[m+3]{\frac{(m+1)A_{pd}P_{ti}\Delta h^{m+1}}{2\pi P_{ri}}} \quad (2)$$

166 where $\Delta h = h_{LED} - z$ is the unknown vertical height difference between
 167 the LED _{i} transmitter and the receiver. Since Δh is unknown, the estimated
 168 distance \hat{d}_i cannot be directly calculated from P_{ri} without knowing Δh , or
 169 equivalently, z . Due to this, a set of estimated distances \hat{d}_i is generated
 170 for different receiver heights, z , ranging from a minimum height h_{min} to
 171 maximum height, $h_{max} \leq h_{LED}$ with 1 mm intervals.

Table 2: Summary of the system parameters

Parameter	Value
Room Width x Length x Height	4 m × 4 m × 4.1 m
Transmitters' Power - P_t	13.3 W, 16.6 W, 16.4 W, 16.1 W
Transmitter's semi-angle - α	60°
Receiver's Height Range - z	0.64 - 2.55 m
Photodetector's Area - A_{pd}	13 mm ²
Receiver's Responsivity	0.22 A/W

172 The measured power of the LEDs can vary from their advertised values
 173 by up to 20%, as demonstrated in [22, 23]. Due to this, we collect one
 174 measurement directly under each transmitter as a calibration step ($\alpha = \beta =$
 175 0). Then the estimated transmitted power is calculated using $P_{ti} = \frac{P_{ri} 2\pi d_i^2}{A_{pd}(m+1)}$
 176 [24]. Table 2 lists the transmitted power for each transmitter.

177 In the case of receiver tilt, the received power will be impacted by an
 178 adapted angle of incidence. In this case, the angle of incidence in (1) is
 179 replaced with:

$$\cos(\beta_{tilt}) = \frac{(x-x_i) \cos(\varphi) \sin(\theta) + (y-y_i) \sin(\varphi) \sin(\theta) + (z-h_{LED}) \cos(\theta)}{d} \quad (3)$$

180 where (x, y, z) are the receiver's coordinates, (x_i, y_i, z_i) are the LED's coordi-
 181 nates, θ is the receiver's tilting angle, which is the angle difference between
 182 the normal vector of the xy-plane and the normal vector of the receiver. φ
 183 is the azimuthal rotation angle, which is the angle difference between the
 184 x-axis and the orthogonal projection of the receiver's normal vector on the
 185 xy-plane.

186 4.2. Positioning Algorithms

187 Two positioning algorithms are used in this paper, CMD and LLS. The
 188 performance of the CMD algorithm is compared with LLS as the latter is
 189 widely adopted in VLP systems.

190 4.2.1. Cayley-Menger Determinant

191 The Cayley-Menger determinant is used in distance geometry for deter-
 192 mining the volume of a triangular pyramid (tetrahedron) based on the dis-
 193 tances between any two of four vertices [25]. Figure 4 (b) shows the position

194 of three points (transmitters), p_1 , p_2 , and p_3 , with p_4 being the unknown
 195 receiver's location.

196 The Cayley-Menger bideterminant of two sequences of n points $[p_1, p_2, \dots, p_n]$
 197 and $[q_1, q_2, \dots, q_n]$ is defined as [26]:

$$D(p_1, \dots, p_n; q_1, \dots, q_n) = 2 \left(\frac{-1}{2} \right)^n \begin{vmatrix} 0 & 1 & 1 & 1 & 1 \\ 1 & D(p_1, q_1) & D(p_1, q_2) & \cdots & D(p_1, q_n) \\ 1 & D(p_2, q_1) & D(p_2, q_2) & \cdots & D(p_2, q_n) \\ \vdots & \vdots & \vdots & \ddots & \vdots \\ 1 & D(p_n, q_1) & D(p_n, q_2) & \cdots & D(p_n, q_n) \end{vmatrix} \quad (4)$$

198 where $D(p_i, q_j)$ is the squared distance between points p_i and q_j . When two
 199 sequences of points are the same (i.e., $p_i = q_i$), then $D(p_1, \dots, p_n; q_1, \dots, q_n)$
 200 is denoted by $D(p_1, \dots, p_n)$ and is simply called CMD [26]. So (4) becomes:

$$D(p_1, p_2, p_3, p_4) = \left(\frac{1}{8} \right) \begin{vmatrix} 0 & 1 & 1 & 1 & 1 \\ 1 & 0 & D(p_1, p_2) & D(p_1, p_3) & D(p_1, p_4) \\ 1 & D(p_1, p_2) & 0 & D(p_2, p_3) & D(p_2, p_4) \\ 1 & D(p_1, p_3) & D(p_2, p_3) & 0 & D(p_3, p_4) \\ 1 & D(p_1, p_4) & D(p_2, p_4) & D(p_3, p_4) & 0 \end{vmatrix} \quad (5)$$

201 with p_4 is the unknown location of the drone, $D(p_4, p_1)$, $D(p_4, p_2)$ and
 202 $D(p_4, p_3)$ are the distances \hat{d}_1 , \hat{d}_2 and \hat{d}_3 that are computed from the RSS
 203 for a given receiver height. It is then possible to calculate the unknown posi-
 204 tion of the receiver (p_4) with respect to three known transmitter coordinates
 205 (p_1, p_2, p_3) using [26]:

$$p_4 = p_1 + k_1 v_1 + k_2 v_2 \pm k_3 (v_1 v_2) \quad (6)$$

where $v_1 = p_2 - p_1$ and $v_2 = p_3 - p_1$, and

$$k_1 = -\frac{D(p_1, p_2, p_3; p_1, p_3, p_4)}{D(p_1, p_2, p_3)}, k_2 = \frac{D(p_1, p_2, p_3; p_1, p_2, p_4)}{D(p_1, p_2, p_3)}, k_3 = \frac{\sqrt{D(p_1, p_2, p_3, p_4)}}{D(p_1, p_2, p_3)}$$

206 The CMD algorithm then outputs $(\hat{x}, \hat{y}, \hat{z})$ for each of the generated pos-
 207 sible heights Δh , and then the cost function is used to estimate the receiver's
 208 height, h , and its corresponding location.

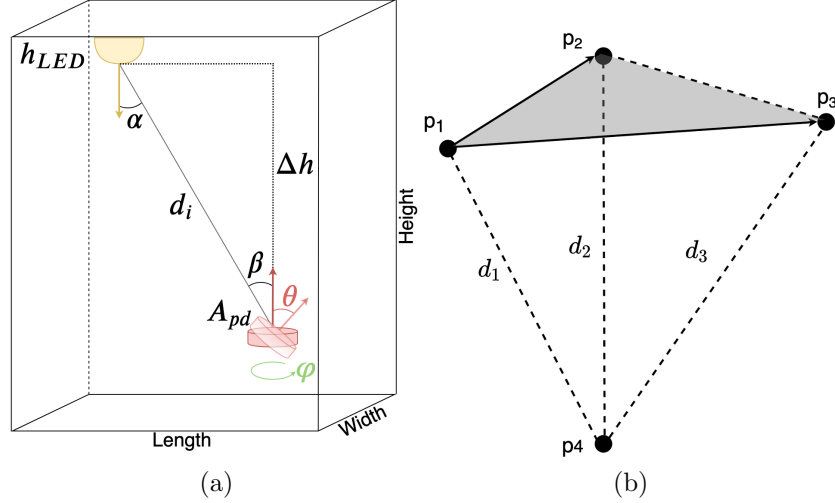


Figure 4: (a) The VLC channel parameters; (b) The parameters of the CMD trilateration algorithm.

209 4.2.2. Linear Least Squares

210 The LLS algorithm is used in this paper as a benchmark for comparison
 211 with the CMD algorithm as it is the most widely adopted trilateration
 212 positioning algorithm in VLP systems [27–29].

213 As the correct distances cannot be estimated directly without knowing
 214 the receiver's height, 2D trilateration using LLS is performed for each of the
 215 generated heights, Δh . The horizontal distance between the LED_i and the
 216 receiver is given by:

$$d_i^2(\Delta h) = (x_i - x)^2 + (y_i - y)^2 = x^2 - 2xx_i + x_i^2 + y^2 - 2yy_i + y_i^2 \quad (7)$$

217 These equations can be expressed in a matrix form as $b=Ax$, where

$$b = \frac{1}{2} \begin{bmatrix} d_1^2(\Delta h) - x_1^2 - y_1^2 - d_N^2(\Delta h) + x_N^2 + y_N^2 \\ d_2^2(\Delta h) - x_2^2 - y_2^2 - d_N^2(\Delta h) + x_N^2 + y_N^2 \\ \vdots \\ d_{N-1}^2(\Delta h) - x_{N-1}^2 - y_{N-1}^2 - d_N^2(\Delta h) + x_N^2 + y_N^2 \end{bmatrix} \quad (8)$$

$$A = \begin{bmatrix} x_1 - x_N & y_1 - y_N \\ x_2 - x_N & y_2 - y_N \\ \vdots & \vdots \\ x_{N-1} - x_N & y_{N-1} - y_N \end{bmatrix}, x = \begin{bmatrix} x \\ y \end{bmatrix} \quad (9)$$

218 The algorithm then outputs the estimated position $\begin{bmatrix} \hat{x} \\ \hat{y} \end{bmatrix}$ for each of the
 219 generated possible heights (Δh) using:

$$x = (A^T A)^{-1} A^T b \quad (10)$$

220 *4.2.3. Cost function*

221 Once all of the possible receiver locations have been generated using (6)
 222 and (10) for both algorithms, the final most probable 3D position of the
 223 receiver is found at the minimum of the cost function $C(h)$ as [19]:

$$C(h) = \frac{1}{N} \sum_{i=1}^N [\hat{d}_i(h) - \sqrt{(\hat{x}(h) - x_i)^2 + (\hat{y}(h) - y_i)^2 + (\hat{z}(h) - z_i)^2}]^2 \quad (11)$$

224 where $C(h)$ is the average squared error between the estimated distances \hat{d}_i
 225 using (2), and the distances of the estimated 3D location of the unknown
 226 receiver calculated using (6) and (10). It should be noted that the cost
 227 function minimization described above can be used in conjunction with any
 228 2D trilateration algorithm [24].

229 The positioning error, which is the distance difference between the final
 230 calculated position and the actual position of the receiver, is calculated using:

$$D_{error} = \sqrt{(\hat{x} - x)^2 + (\hat{y} - y)^2 + (\hat{z} - z)^2} \quad (12)$$

231 where $z = h$. The CMD algorithm only requires three signals to estimate the
 232 receiver's position while the LLS generally utilizes all the received signals.
 233 In our experiment, the LLS algorithm in (8) is restricted to use only the
 234 strongest three signals to ensure a fair comparison. Also, restricting the LLS
 235 to use only the strongest signals has been shown to increase the positioning
 236 accuracy and lessen the impact of multipath reflection [30, 31]. The cost
 237 function on the other hand uses all four signals from the LEDs for the mini-
 238 mization, as three LEDs do not suffice for an unambiguous 3D localization.

239 5. Results

240 The performance of the algorithms is experimentally evaluated for dif-
 241 ferent parameters in terms of positioning error while considering different
 242 realistic factors: (i) different LED configurations, (ii) different receiver tilt
 243 angles, and (iii) introduced multipath reflection through the inclusion of a
 244 storage rack. Moreover, the results section also examines the performance
 245 of the algorithms for a 2D system. In this case, the height of the receiver is
 246 assumed to be exactly known through the use of an additional sensor.

247 5.1. Positioning Accuracy for Untilted Receiver

248 5.1.1. Square Configuration

249 Figure 5 (a) shows the CDF using the CMD and LLS algorithms for a
 250 2D and 3D positioning system. The median (p_{50}) and maximal (p_{90}) 2D
 251 errors recorded using the LLS algorithm are 11.7 cm and 26.7 cm, while
 252 these are 9.9 cm and 15.8 cm using the CMD algorithm. In a 3D system,
 253 the measured median error is 17.1 cm and the maximal error is 88.4 cm
 254 for the LLS algorithm while the CMD algorithm achieves a median error of
 255 55.9 cm and a maximal error of 177.9 cm. The positioning errors for the 2D
 256 estimation are much smaller than the 3D estimation. This is due to the height
 257 being known to the receiver, avoiding the need for the cost function and
 258 eliminating the 3D positioning ambiguity [19]. In the case of 2D positioning,
 259 the CMD outperforms the LLS algorithms slightly while the LLS algorithm
 260 outperforms the CMD algorithm in a 3D system. However, the 3D estimation
 261 for both algorithms is unreliable due to the high positioning errors under the
 262 square configuration. This is caused by the position ambiguity in a square
 263 configuration as expected and further analyzed in our previous work [19, 24].
 264 The issue arises because some locations in the room have the same received
 265 power values, and distances once converted, as other locations, which occurs
 266 due to the radiation pattern's geometrical properties [32].

267 5.1.2. Star Configuration

268 Figure 5 (b) shows the CDF of the positioning errors using the star ar-
 269 rangement of LEDs for both 2D and 3D position estimation. The overall
 270 error values have decreased noticeably when compared with the square ar-
 271 rangement as the position ambiguity is not present in the star configuration.
 272 The performance of the LLS and CMD algorithms are very similar for the

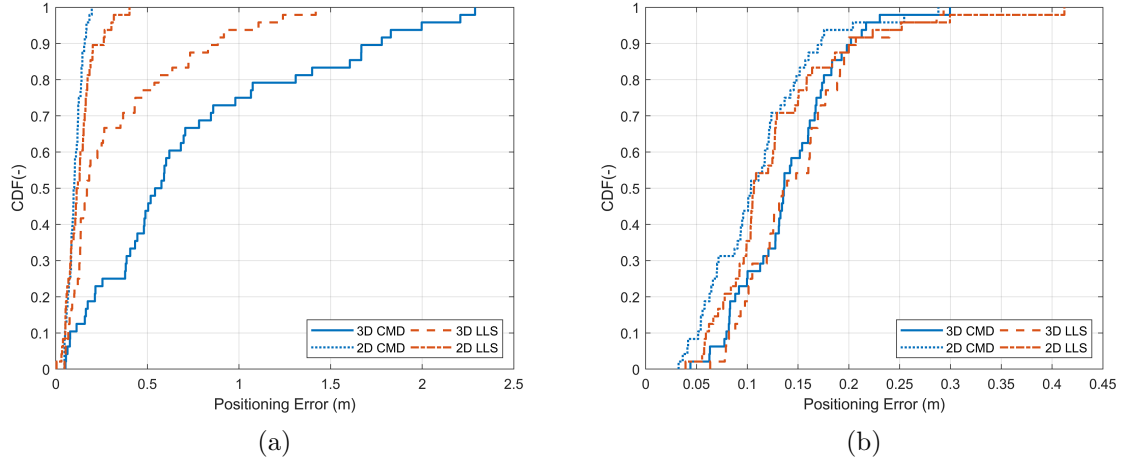


Figure 5: The CDF of the 2D and 3D positioning errors for both algorithms with a parallel receiver. (a) Under a square LED configuration; (b) Under a star LED configuration.

273 3D system with the median and maximal errors achieved using the LLS al-
 274 gorithm are 10.6 cm & 24.9 cm, and 10.5 cm & 21.1 cm using the CMD
 275 algorithm, respectively. In the case of the 2D system, median and maximal
 276 positioning errors of 8 and 25.2 cm were measured using the LLS algorithm
 277 and 6.7 cm & 14.6 cm using the CMD algorithm. Note that most of the
 278 large errors occurred at heights of more than 2 meters as can be seen in
 279 Figure 6, which depicts the estimated 3D paths and shows a deviation when
 280 the receiver is over 2 meters.

281 *5.2. Positioning Accuracy for a tilted receiver*

282 The errors introduced by the receiver tilt are due to the assumption in
 283 (2) that the transmitters' and receiver's plane are perfectly parallel to each
 284 other. This assumption is widely adopted due to its simplicity. However, it
 285 is unrealistic as it is almost impossible to achieve perfectly parallel planes
 286 in real-life settings, as even a 1° difference can increase the positioning error
 287 [33]. This is especially important when considering the use of a VLP system
 288 with aerial receivers, as they tilt for movement. Therefore, the effect of tilting
 289 on the performance of positioning algorithms is investigated here.

290 To accurately assess the effect of the receiver's tilt, the receiver is mounted

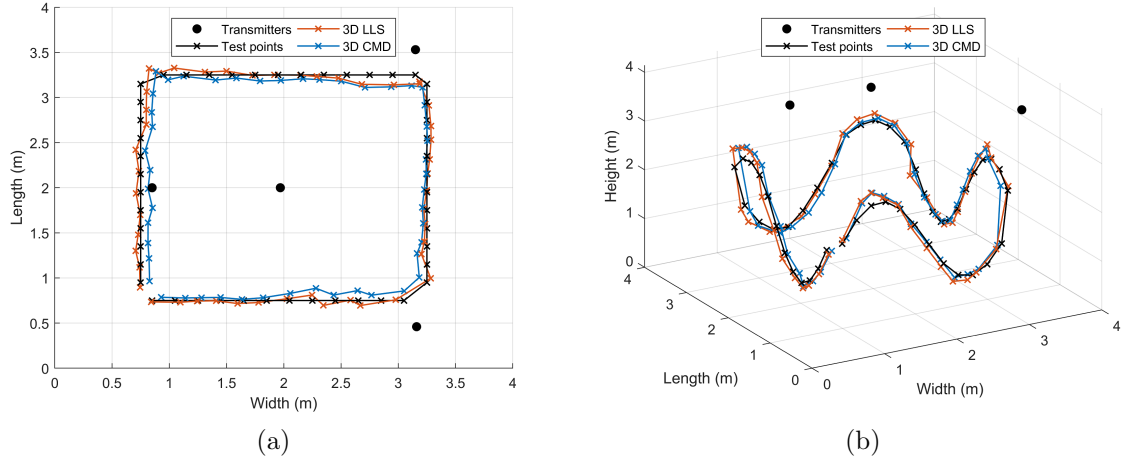


Figure 6: An illustration of the estimated paths under a star configuration when the receiver is parallel. (a) A top-view of the test points and the estimated 3D positions using the LLS and CMD algorithms; (b) a 3D view of the test points and the estimated points.

291 on a Thorlabs GNL10/M² goniometer with a range of $\pm 10^\circ$ and a precision
 292 of 1° as shown in the inset of Figure 1 (b). Two tilt angles of 5° and 10°
 293 are considered and investigated. The tilt of the receiver is set to a forward tilt
 294 angle, meaning that the receiver is always facing the direction of movement
 295 along the path outlined earlier in Section 3 and shown in Figure 2 (a). The
 296 forward tilt is introduced here because UAVs normally tilt forward to move.

297 5.2.1. Square Configuration

298 Figure 7 (a) shows the CDF of the positioning errors using the square-
 299 shaped LED configuration for both 2D and 3D estimation with a receiver
 300 tilt angle $\theta = 5^\circ$. The measured median and maximal errors using the LLS
 301 algorithm were 9.5 cm and 17.8 cm, and it is 8.8 cm and 15.3 cm when
 302 the CMD algorithm is used. In a 3D system, the median and maximal
 303 errors for 2D using the LLS algorithm are 17.4 and 76.9 cm, while it is 62.9
 304 and 177.5 cm when the CMD algorithm is used. The results show that LLS
 305 outperforms the CMD algorithm in a square configuration. Figure 7 (c) shows
 306 the performance of the system with a receiver tilt of 10° . For a 2D system,

²<https://www.thorlabs.com/thorproduct.cfm?partnumber=GNL10/M>

Table 3: A summary of the experimentally obtained median and maximal positioning errors for the two LED configurations for 2D and 3D localization when the receiver has a tilt of 0° , 5° , and 10° .

Positioning Error(cm)	2D LLS		2D CMD		3D LLS		3D CMD	
	P_{50}	P_{90}	P_{50}	P_{90}	P_{50}	P_{90}	P_{50}	P_{90}
Square ($\theta = 0^\circ$)	11.7	26.2	9.9	15.8	17.1	88.4	55.9	177.9
Star ($\theta = 0^\circ$)	8	25.2	6.7	14.6	10.6	24.9	10.5	21.1
Square ($\theta = 5^\circ$)	9.5	17.8	8.8	15.3	17.4	76.9	62.9	177.5
Star ($\theta = 5^\circ$)	10.7	20.7	10.4	17.3	13.7	20	13.6	20.2
Square ($\theta = 10^\circ$)	19.4	28.1	15.6	22.8	27.1	186.4	106.7	181.8
Star ($\theta = 10^\circ$)	23.2	36.3	18.8	31.3	22.7	32.2	21.6	34.2

307 the recorded median errors are 19.4 and 15.6 cm for the LLS and CMD
 308 algorithms, respectively. The largest errors recorded are when a 3D system
 309 was used with a receiver tilt $\theta = 10^\circ$ with a median of 27.1 cm using LLS,
 310 and 106.7 cm using CMD. These results again demonstrate the unreliability
 311 of using a square layout when implementing the algorithm. Table 3 lists a
 312 summary of the obtained accuracies across all tilt angles for the CMD and
 313 LLS algorithms under the two LED configurations.

314 5.2.2. Star Configuration

315 Figure 7 (b) shows the CDF of the positioning error for the entire path
 316 when the receiver is tilted by $\theta = 5^\circ$ under a star configuration. When the
 317 LLS algorithm is used for 3D positioning, the median error is 13.7 cm and
 318 the maximal error is 20 cm. In the case of 2D positioning, the median error
 319 is 10.7 cm and the maximal error is 20.7 cm, which is slightly better than
 320 3D positioning. When the CMD algorithm is used for 2D positioning, the
 321 median and maximal errors recorded were 10.4 and 17.3 cm, and in the case
 322 of 3D positioning, the median and maximal errors are 13.6 and 20.2 cm.

323 The measured positioning errors with $\theta = 10^\circ$ are shown in Figure 7 (d).
 324 Median and maximal errors for the 2D system are 23.2 cm and 36.3 cm for
 325 the LLS algorithm, while it is 18.8 cm and 31.3 cm for the CMD algorithm,
 326 respectively. In a 3D positioning system, the median and maximal errors
 327 were 22.7 cm and 32.2 cm when using the LLS algorithm, and 21.6 cm and
 328 34.2 cm using the CMD algorithm.

329 In can be noticed that some of the errors are higher under a square setting
 330 with an untilted receiver than when the receiver is $\theta = 5^\circ$, see Table 3. The
 331 increase is due to some of the measured samples having large errors that
 332 have skewed the maximal errors. Note that, the tilt effect could be alleviated

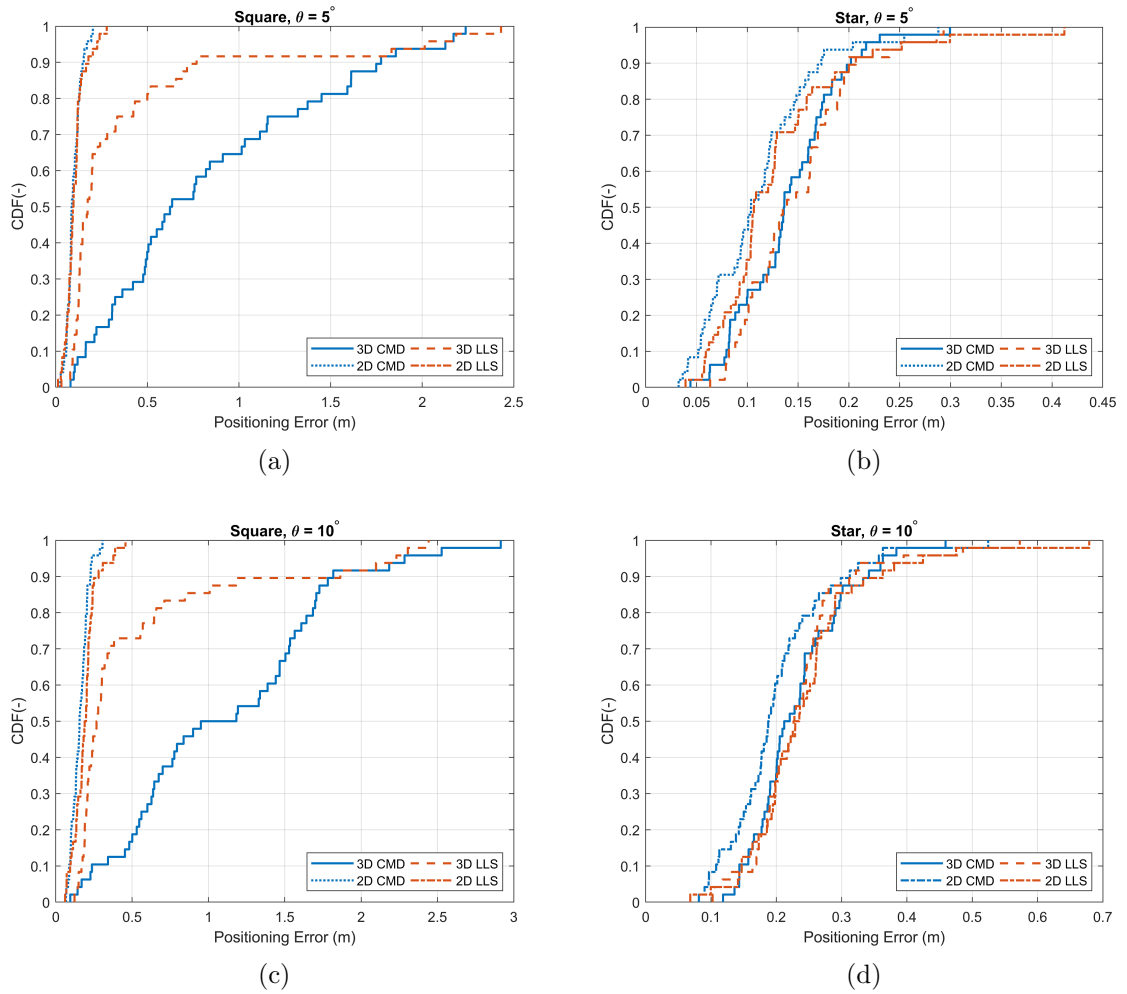


Figure 7: The CDF of the 2D and 3D positioning errors for both algorithms with receiver tilt, θ . (a) Square LED configuration with a receiver tilt of 5° ; (b) Star LED configuration with a receiver tilt of 5° ; (c) Square LED configuration with a receiver tilt of 10° ; (d) Star LED configuration with a receiver tilt of 10° .

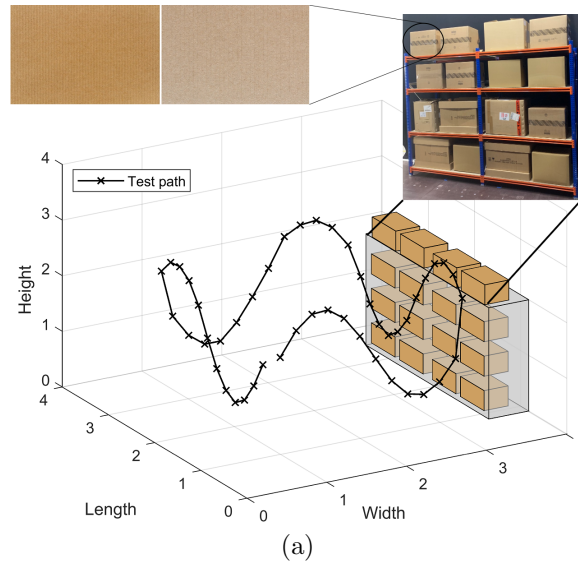


Figure 8: A 3D view of the storage rack and test path in relation to the room. The inset shows the storage rack stocked with boxes with reflectivity of 33% and 42% depending on color tone.

333 through compensating its value, which can be performed by receivers that
 334 are equipped with an IMU/gyroscope [34, 35] or with algorithms such as
 335 simultaneous positioning and orientating (SPA0) [36].

336 5.3. Positioning Accuracy in the Presence of Multipath Reflections

337 Industrial environments are one of the areas where an indoor positioning
 338 system could prove valuable. As discussed previously, UAVs and AGVs can
 339 be deployed in warehouses and storage facilities with the help of VLP systems
 340 for inventory management applications. In order to replicate an industrial
 341 warehouse, a metal storage rack was added to the room as shown in Figure 2.
 342 The rack is placed at one side of the room along the path and is stocked with
 343 different-sized boxes as shown in the inset of Figure 8. The height of the
 344 storage rack is 2 m and measures 2.36 m when stocked with boxes and has a
 345 length of 2.66 m. The storage rack is placed 26 cm away from the path test
 346 points that runs parallel to it. A 3D illustration of the storage rack and the
 347 test points in the room can be seen in Figure 8.

348 Research work has shown that reflections degrade the performance of
 349 VLP systems, especially when near highly reflective surfaces such as white
 350 painted walls that have a reflectivity of around 70% [30]. In our case, the

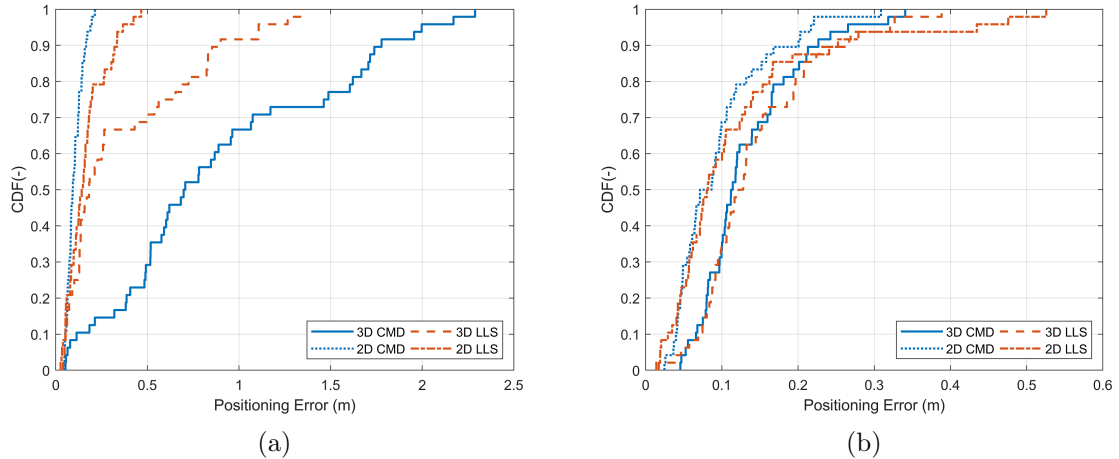


Figure 9: The CDF of the 2D and 3D positioning errors for both algorithms with a parallel receiver in the presence of a storage rack. (a) Under a square LED configuration; (b) and under a star LED configuration.

351 reflectivity of the boxes ranges between 33-42% depending on the color tone
 352 of the cardboard as demonstrated in the inset of Figure 8. These values were
 353 obtained using DIALux³. The same measurement procedure and scenarios
 354 outlined earlier (two LED configurations with 2D and 3D using the CMD and
 355 LLS trilateration algorithms) have been repeated, and then the positioning
 356 error was calculated using (12).

357 5.3.1. Untilted Receiver

358 Figure 9 (a) shows the CDF of the positioning errors using a square
 359 configuration with the inclusion of the storage rack. In the 2D system, the
 360 median and maximal errors using the LLS algorithm are 14.5 cm and 33.4 cm,
 361 whereas the CMD algorithm achieve a median and maximal value of 9.3 cm
 362 and 16.5 cm using the CMD algorithm.

363 Figure 9 (b) shows the CDF of the positioning errors using the LLS and
 364 CMD algorithms under a star LED configuration. The median and maximal
 365 2D errors using the LLS algorithm are 8.1 cm and 25.2 cm, whereas a median
 366 error of 7.9 cm and a maximal error of 20.1 cm when the CMD algorithm is

³<https://www.dial.de/en/dialux/>

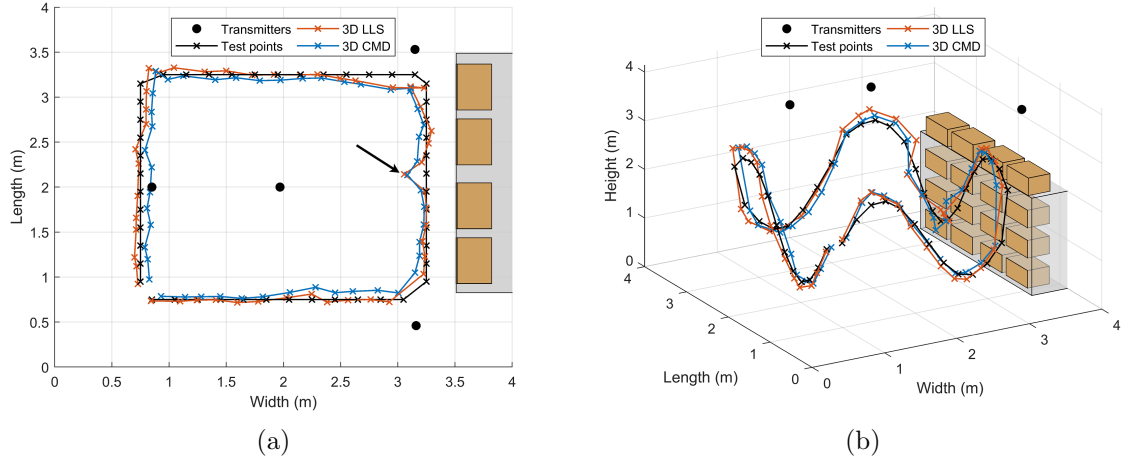


Figure 10: (a) A top-view of the test points and the estimated 3D positions using the LLS and CMD algorithms when the receiver is parallel; (b) a 3D view of the test points and the estimated 3D points.

367 used. The errors increase slightly in a 3D system with median and maximal
 368 errors of 12.5 cm and 26.7 cm using the LLS algorithm. In a 3D system,
 369 the CMD algorithm achieved a median and a maximal value of 11.3 cm and
 370 22.7 cm.

371 Figure 10 illustrates the estimated paths using the CMD and LLS algo-
 372 rithms. The errors on the right side and top-right side near the storage rack
 373 are due to reflections from the boxes and the metal rods [37]. The bottom-
 374 right path is not particularly affected as some receiver heights are higher
 375 than the storage rack. Figure 10 (a) demonstrates the detrimental impact of
 376 reflections for the points that run parallel to the storage rack. One particular
 377 point directly across the metal rod is heavily affected by the multipath reflection
 378 emanating from the central LED and as highlighted in Figure 10 (a).
 379 The positioning error for that point in the 3D systems reported an error of
 380 19.7 cm using the LLS algorithm, increasing from 6.7 cm when the point was
 381 calculated prior to adding a storage rack. Using the CMD algorithm, that
 382 specific point reported an error of 26.6 cm, whereas it was 8.6 cm prior to the
 383 addition of the storage rack. Overall, the results do not differ greatly when
 384 compared with the results in the absence of the storage rack except for the
 385 points that are nearest to storage rack.

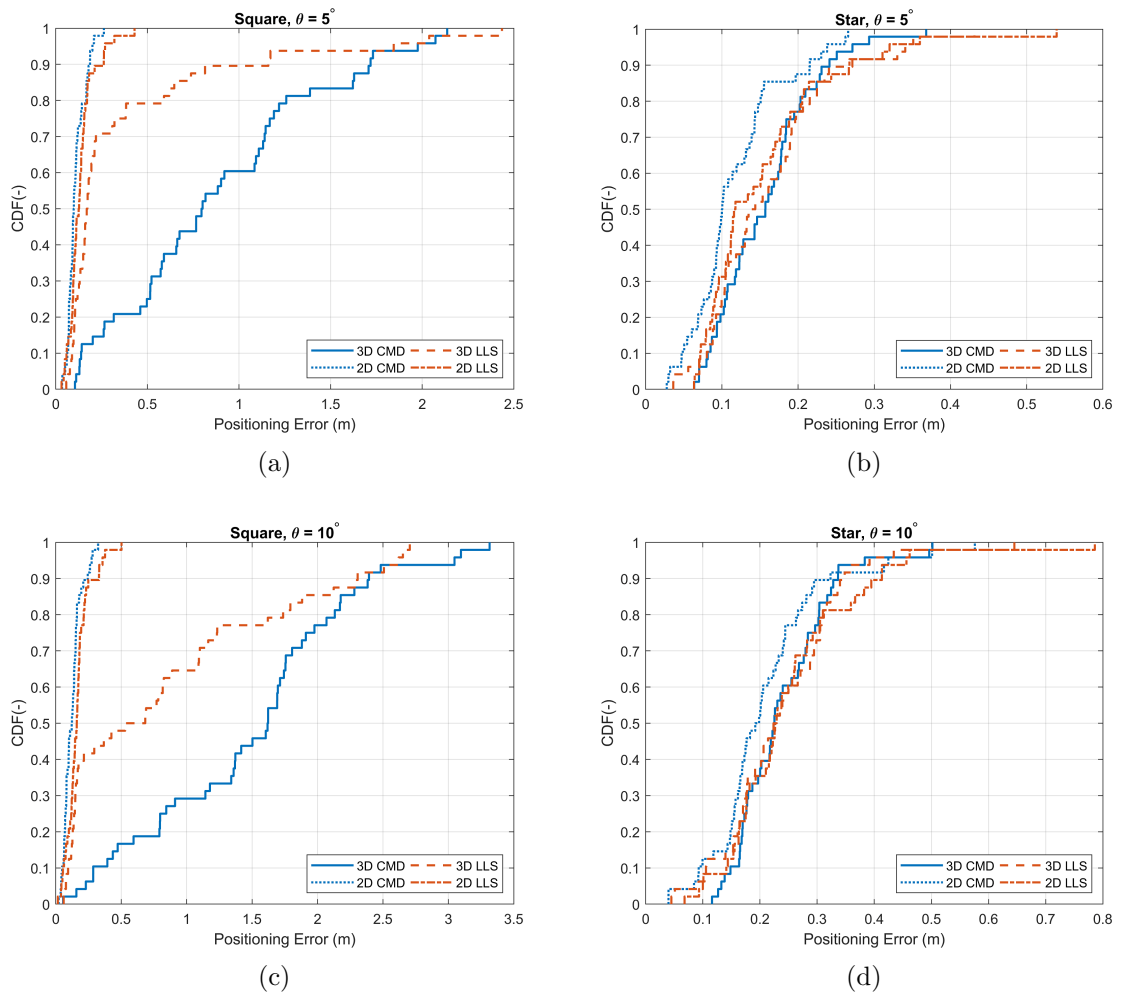


Figure 11: The CDF of the 2D and 3D positioning errors for both algorithms when the receiver is tilted and with the inclusion of a storage rack. (a) Square configuration with a receiver tilt of 5° ; (b) Star configuration with a receiver tilt of 5° ; (c) Square configuration with a tilt of 10° ; (d) Star configuration with a receiver tilted 10° .

Table 4: A summary of the experimentally obtained median and maximal positioning errors for the two LED configurations for 2D and 3D localization when the receiver has a tilt of 0° , 5° , and 10° in the presence of a storage rack.

Positioning Error (cm)	2D LLS		2D CMD		3D LLS		3D CMD	
	P_{50}	P_{90}	P_{50}	P_{90}	P_{50}	P_{90}	P_{50}	P_{90}
Square ($\theta = 0^\circ$)	14.5	33.4	9.3	16.5	18.2	90	70.2	177.8
Star ($\theta = 0^\circ$)	8.1	25.2	7.9	20.1	12.2	26.7	11.3	22.7
Square ($\theta = 5^\circ$)	12.6	26.2	9.8	18.7	17.1	116	79.8	171.8
Star ($\theta = 5^\circ$)	11.7	26.7	10	21.5	13.9	27.1	15.7	24.1
Square ($\theta = 10^\circ$)	16	33	12.3	24.4	60.7	230.7	162	239.3
Star ($\theta = 10^\circ$)	22.8	41.3	19.5	32.3	22.5	34.8	22.5	33.7

386 5.3.2. Tilted Receiver

387 Similar to Subsection 5.2, the measurements are repeated with the re-
 388 ceiver tilted by 5° and 10° . This means that the system/receiver will suffer
 389 from both the effects of tilt and multipath reflections. Figure 11 shows the
 390 CDF of the positioning errors when the receiver is tilted 5° and 10° for both
 391 LED configurations. Under a square setting and when the receiver is tilted
 392 by 5° , the measured median and maximal 2D errors using the LLS algorithm
 393 were 12.6 and 26 cm, whereas it is 9.8 cm and 18.7 cm when the CMD al-
 394 gorithm is used, see Figure 11 (a). In the 3D system, the measured median
 395 and maximal values are 17.1 cm and 116 cm using the LLS algorithm. Using
 396 the CMD algorithm achieved 3D median and maximal values of 79.8 and
 397 171.8 cm. Here, the results show that 70% of the errors in a 3D system using
 398 the LLS algorithm are below 22 cm, as shown in Figure 11 (a).

399 In the 2D system when the receiver is tilted by 10° , the LLS algorithm
 400 achieved median and maximal errors of 16 and 33 cm. While the CMD
 401 algorithm achieved median and maximal values of 12.3 and 24.4 cm. In the
 402 3D system, the LLS algorithm reported a median of 60.7 cm and using the
 403 CMD algorithm reported 1.62 m as shown in Figure 11 (c). As expected, the
 404 errors increase when the tilt is increased to 10° .

405 Figure 11 (b) demonstrates the CDF for a receiver with a tilt of 5° under
 406 the star arrangement. Using the LLS algorithm, the achieved 2D median
 407 and maximal errors are 11.7 cm and 26.7 cm, whereas they are 10 cm and
 408 21.5 cm when the CMD algorithm is used. For the 3D positioning system, the
 409 median error using the LLS algorithm is 13.9 cm, an increase of 13.9% when
 410 compared with an untilted receiver. Using the CMD algorithm, the median
 411 is 15.7 cm, increasing by 39% to when the receiver was untilted. When

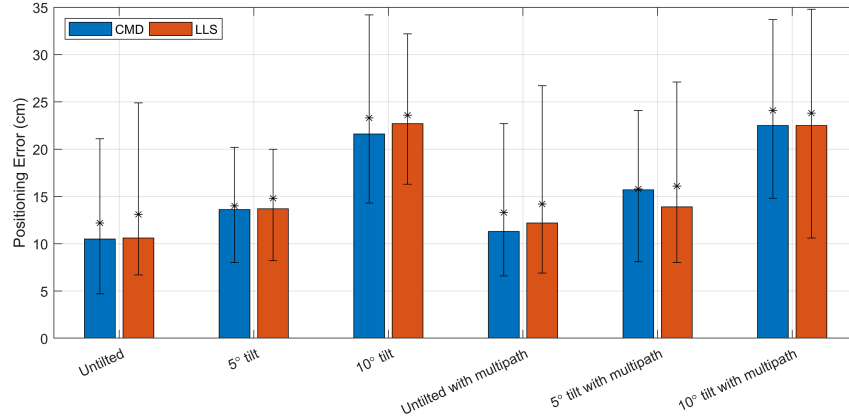


Figure 12: The bars show the achieved 3D median errors using the CMD and LLS trilateration algorithms under a star configuration, the error bars show the 10% and 90% quantiles, and the asterisks represent the mean error.

412 the tilt is 5° , the CMD algorithm outperforms the LLS algorithm when it
 413 comes to 2D positioning. The results, however, are nearly identical in the
 414 3D positioning system.

415 When the receiver’s tilt is set to 10° under a star arrangement, the per-
 416 formance of the two algorithms in both 2D and 3D positioning system are
 417 similar. The median 3D error reported 22.5 cm for both algorithms, see
 418 Figure 11. Table 4 lists a summary of the obtained accuracies across all
 419 tilt angles in the presence of the storage rack. Compared to when the re-
 420 ceiver was untilted, the errors increased by 84% using the LLS algorithm and
 421 doubled when using the CMD algorithm.

422 6. Discussion

423 We experimentally evaluated and compared two different VLP trilater-
 424 ation algorithms in a $4\text{ m} \times 4\text{ m} \times 4.1\text{ m}$ room under two different LED
 425 configurations for both 2D and 3D systems. The performances of the algo-
 426 rithms were also examined in the presence of a storage rack to examine the
 427 effects of multipath reflections. Our experiments demonstrated the imprac-
 428 ticality of using a square-shaped configuration and showed the higher posi-
 429 tioning accuracy of a star-shaped configuration. Previous simulation work
 430 identified an issue when the LEDs were placed in a square configuration [19].

431 Therefore, a star-shaped configuration was proposed. This shortcoming was
 432 experimentally examined in this paper.

433 The results under a star configuration were highly more accurate com-
 434 pared to the square configuration. The 3D median error achieved using LLS
 435 and CMD were 10.6 cm and 10.5 cm, respectively. When a tilt of 5° was in-
 436 troduced, the 3D median errors increased slightly to 13.7 cm and 13.6 cm for
 437 LLS and CMD, an increase of 29.3% and 29.5%. A tilt of 10° increased the
 438 3D median errors of LLS and CMD to 22.7 cm and 21.6 cm, corresponding to
 439 an increase of 114.2% and 106% when compared with a horizontal receiver.
 440 From these results, we can conclude that the positioning error increases by
 441 around 30% if the receiver is tilted by 5° , and essentially doubles when the
 442 receiver is tilted by 10° . Figure 12 shows the median errors for all of the
 443 considered scenarios under a star arrangement, the error bars show the 10%
 444 and 90% quantiles, and the asterisks show the mean error. A slight difference
 445 in terms of positioning error between the median and mean can be seen for
 446 some of the scenarios.

447 The effect of multipath reflections on the performance of VLP systems
 448 was also examined. A metallic storage rack filled with boxes was added in
 449 the evaluated room and tested with a horizontal receiver with a receiver
 450 tilt of 5° and 10° . The results for a 3D system under a star configuration
 451 reported a median error of 12.2 cm using LLS, an increase of 15% when com-
 452 pared with an empty room. Using the CMD algorithm, the median error was
 453 11.3 cm, which represents an increase of 7.6% compared to its performance
 454 in an empty room. The storage rack was 26 cm away from the closest points
 455 and the impact of reflections on one particular point (pointed out in Figure
 456 10) increased the positioning error in a 3D system using the LLS algorithm
 457 by 13 cm, and by 18 cm using the CMD algorithm [37]. This points out
 458 the severity of multipath reflections from metallic structures. As mentioned
 459 before, both algorithms in this paper select the three strongest signals to
 460 increase the positioning accuracy and lessen the impact of multipath reflec-
 461 tions as noted in [30, 31]. However, while the impact of reflections may have
 462 been reduced, it is still not sufficient enough in limiting the degrading effect
 463 of reflections.

464 The differences in the performances of the algorithms are because they
 465 differ mathematically in how they calculate the receiver's position. The CMD
 466 method is an analytic procedure, that calculates a point through geometric
 467 interrelations [38]. Whereas the least square method is a numeric procedure
 468 that calculates the point at which the distance from three circles intersects.

469 The observation that the CMD trilateration algorithm outperforms the least
470 square quadratic method has also been noted by researchers in [39] when
471 they compared different trilateration algorithms.

472 It should be noted that some of the errors observed in the experiments
473 could also be caused by other factors. The experimentally adjusted tilt an-
474 gle can be slightly different from the intended values, the LED having small
475 unknown tilt angles [33], the LED radiation pattern not being perfectly Lam-
476 bertian, and imperfections in the demultiplexing process.

477 7. Conclusion

478 In this paper, two VLP algorithms were experimentally analyzed and
479 compared. The LLS and CMD algorithms were tested in a $4\text{ m} \times 4\text{ m} \times 4.1\text{ m}$
480 room with four LEDs. Two different LED configurations were compared
481 using two different trilateration algorithms and their 2D and 3D performances
482 were evaluated. The LLS and CMD algorithms achieved an accuracy of
483 10.6 and 10.5 cm in a 3D system, respectively. The performances of the
484 algorithms were also examined in the presence of a storage rack to examine
485 the effects of multipath reflections. We also experimentally demonstrated the
486 impracticality of using a square-shaped configuration and showed the higher
487 positioning accuracy of a star-shaped configuration. The proposed algorithm
488 is suitable for real-time implementation based on our previous work reporting
489 a computation time of 17 ms, which can be further reduced to less than 2 ms
490 using a fast search algorithm [19].

491 The presented work highlights the need to take into account the light
492 arrangements to optimize the performance of a 3D VLP system as well as
493 the effect of receiver tilt and multipath reflections on the performance of
494 VLP systems. It also extended the use of a trilateration algorithm that is
495 not widely used into VLP systems. Future work could examine integrating
496 an IMU sensor to compensate for the undesirable effects of tilt. Additional
497 plans could also investigate the performance of the algorithm under a circular
498 LED arrangement as the work in [40] reported that a circular arrangement
499 offers a slightly higher illuminance uniformity than the optimum condition
500 using rectangular LED arrangement.

501 Acknowledgments

502 The authors would like to thank Willem Raes and Nobby Stevens of
503 DRAMCO, ESAT, KU LEUVEN, Belgium for providing the LED modules

504 used in this work.

505 **Funding Information**

506 This research received no external funding.

507 **References**

- 508 [1] R. Xu, W. Chen, Y. Xu, S. Ji, A new indoor positioning sys-
509 tem architecture using GPS signals, *Sensors* 15 (2015) 10074–10087.
510 doi:10.3390/s150510074.
- 511 [2] F. Zafari, A. Gkelias, K. K. Leung, A survey of indoor localization
512 systems and technologies, *IEEE Communications Surveys Tutorials* 21
513 (2019) 2568–2599. doi:10.1109/COMST.2019.2911558.
- 514 [3] H. Burchardt, N. Serafimovski, D. Tsonev, S. Videv, H. Haas, Vlc: Be-
515 yond point-to-point communication, *IEEE Communications Magazine*
516 52 (2014) 98–105.
- 517 [4] X. Guo, S. Shao, N. Ansari, A. Khreishah, Indoor localization using
518 visible light via fusion of multiple classifiers, *IEEE Photonics Journal* 9
519 (2017) 1–16. doi:10.1109/JPHOT.2017.2767576.
- 520 [5] Y. Cai, W. Guan, Y. Wu, C. Xie, Y. Chen, L. Fang, Indoor high pre-
521 cision three-dimensional positioning system based on visible light com-
522 munication using particle swarm optimization, *IEEE Photonics Journal*
523 9 (2017) 1–20. doi:10.1109/JPHOT.2017.2771828.
- 524 [6] C. Hsu, S. Liu, F. Lu, C. Chow, C. Yeh, G. Chang, Accurate indoor
525 visible light positioning system utilizing machine learning technique with
526 height tolerance, in: *2018 Optical Fiber Communications Conference*
527 *and Exposition (OFC)*, 2018, pp. 1–3.
- 528 [7] Z. Xie, W. Guan, J. Zheng, X. Zhang, S. Chen, B. Chen, A high-
529 precision, real-time, and robust indoor visible light positioning method
530 based on mean shift algorithm and unscented Kalman filter, *Sensors* 19
531 (2019). doi:10.3390/s19051094.

- 532 [8] H. Zhang, J. Cui, L. Feng, A. Yang, H. Lv, B. Lin, H. Huang, High-
533 precision indoor visible light positioning using deep neural network based
534 on the Bayesian regularization with sparse training point, *IEEE Pho-*
535 *tonics Journal* 11 (2019) 1–10. doi:10.1109/JPHOT.2019.2912156.
- 536 [9] P. Du, S. Zhang, C. Chen, A. Alphones, W. Zhong, Demonstration
537 of a low-complexity indoor visible light positioning system using an
538 enhanced TDOA scheme, *IEEE Photonics Journal* 10 (2018) 1–10.
539 doi:10.1109/JPHOT.2018.2841831.
- 540 [10] S. Zhang, W. Zhong, P. Du, C. Chen, Experimental demonstra-
541 tion of indoor sub-decimeter accuracy VLP system using differential
542 PDOA, *IEEE Photonics Technology Letters* 30 (2018) 1703–1706.
543 doi:10.1109/LPT.2018.2866402.
- 544 [11] Z. Li, L. Feng, A. Yang, Fusion based on visible light positioning and
545 inertial navigation using extended Kalman filters, *Sensors* 17 (2017).
546 doi:10.3390/s17051093.
- 547 [12] L. Li, P. Hu, C. Peng, G. Shen, F. Zhao, Epsilon: A visible light
548 based positioning system, in: *11th USENIX Symposium on Networked*
549 *Systems Design and Implementation (NSDI 14)*, USENIX Association,
550 Seattle, WA, 2014, pp. 331–343.
- 551 [13] M. Yasir, S. Ho, B. N. Vellambi, Indoor positioning system using visible
552 light and accelerometer, *Journal of Lightwave Technology* 32 (2014)
553 3306–3316. doi:10.1109/JLT.2014.2344772.
- 554 [14] S. Yang, H. Kim, Y. Son, S. Han, Three-dimensional visible
555 light indoor localization using aoa and rss with multiple optical
556 receivers, *Journal of Lightwave Technology* 32 (2014) 2480–2485.
557 doi:10.1109/JLT.2014.2327623.
- 558 [15] W. Guan, S. Chen, S. Wen, Z. Tan, H. Song, W. Hou, High-accuracy
559 robot indoor localization scheme based on robot operating system using
560 visible light positioning, *IEEE Photonics Journal* 12 (2020) 1–16.
- 561 [16] W. Guan, X. Zhang, Y. Wu, Z. Xie, J. Li, J. Zheng, High precision
562 indoor visible light positioning algorithm based on double leds using
563 cmos image sensor, *Applied Sciences* 9 (2019). doi:10.3390/app9061238.

- 564 [17] Y. Almadani, M. Ijaz, W. Joseph, S. Bastiaens, S. Rajbhandari, B. Ade-
565 bisi, D. Plets, A novel 3d visible light positioning method using re-
566 ceived signal strength for industrial applications, *Electronics* 8 (2019).
567 doi:10.3390/electronics8111311.
- 568 [18] S. De Lausnay, L. De Strycker, J. Goemaere, N. Stevens, B. Nauwelaers,
569 A visible light positioning system using frequency division multiple ac-
570 cess with square waves, in: 2015 9th International Conference on Sig-
571 nal Processing and Communication Systems (ICSPCS), 2015, pp. 1–7.
572 doi:10.1109/ICSPCS.2015.7391787.
- 573 [19] D. Plets, Y. Almadani, S. Bastiaens, M. Ijaz, L. Martens, W. Joseph,
574 Efficient 3d trilateration algorithm for visible light positioning, *Journal*
575 *of Optics* 21 (2019) 05LT01. doi:10.1088/2040-8986/ab1389.
- 576 [20] J. M. Kahn, J. R. Barry, *Wireless infrared communications*, *Proceedings*
577 *of the IEEE* 85 (1997) 265–298. doi:10.1109/5.554222.
- 578 [21] Y. Almadani, M. Ijaz, S. Rajbhandari, U. Raza, B. Adebisi, Applica-
579 tions of visible light communication for distance estimation: a short sur-
580 vey, in: 2019 IEEE Jordan International Joint Conference on Electrical
581 Engineering and Information Technology (JEEIT), 2019, pp. 261–265.
582 doi:10.1109/JEEIT.2019.8717459.
- 583 [22] D. Plets, S. Bastiaens, L. Martens, W. Joseph, N. Stevens, On the
584 impact of led power uncertainty on the accuracy of 2d and 3d visible light
585 positioning, *Optik* 195 (2019) 163027. doi:10.1016/j.ijleo.2019.163027.
- 586 [23] D. Plets, S. Bastiaens, N. Stevens, L. Martens, W. Joseph, Monte-carlo
587 simulation of the impact of led power uncertainty on visible light posi-
588 tioning accuracy, in: 2018 11th International Symposium on Commu-
589 nication Systems, Networks Digital Signal Processing (CSNDSP), 2018,
590 pp. 1–6. doi:10.1109/CSNDSP.2018.8471838.
- 591 [24] D. Plets, S. Bastiaens, M. Ijaz, Y. Almadani, L. Martens, W. Raes,
592 N. Stevens, W. Joseph, Three-dimensional visible light positioning: an
593 experimental assessment of the importance of the leds’ locations, in:
594 2019 International Conference on Indoor Positioning and Indoor Navi-
595 gation (IPIN), 2019, pp. 1–6. doi:10.1109/IPIN.2019.8911763.

- 596 [25] Z. Jia, C. Wu, Z. Li, Y. Zhang, B. Guan, The indoor local-
597 ization and tracking estimation method of mobile targets in three-
598 dimensional wireless sensor networks, *Sensors* 15 (2015) 29661–29684.
599 doi:10.3390/s151129661.
- 600 [26] F. Thomas, L. Ros, Revisiting trilateration for robot local-
601 ization, *IEEE Transactions on Robotics* 21 (2005) 93–101.
602 doi:10.1109/TRO.2004.833793.
- 603 [27] T.-H. Do, M. Yoo, An in-depth survey of visible light communication
604 based positioning systems, *Sensors* 16 (2016). doi:10.3390/s16050678.
- 605 [28] Y. Zhuang, L. Hua, L. Qi, J. Yang, P. Cao, Y. Cao, Y. Wu, J. Thomp-
606 son, H. Haas, A survey of positioning systems using visible led
607 lights, *IEEE Communications Surveys Tutorials* 20 (2018) 1963–1988.
608 doi:10.1109/COMST.2018.2806558.
- 609 [29] J. Luo, L. Fan, H. Li, Indoor positioning systems based on visible
610 light communication: State of the art, *IEEE Communications Surveys
611 Tutorials* 19 (2017) 2871–2893. doi:10.1109/COMST.2017.2743228.
- 612 [30] W. Gu, M. Aminikashani, P. Deng, M. Kavehrad, Impact of multi-
613 path reflections on the performance of indoor visible light position-
614 ing systems, *Journal of Lightwave Technology* 34 (2016) 2578–2587.
615 doi:10.1109/JLT.2016.2541659.
- 616 [31] W. Tang, J. Zhang, B. Chen, Y. Liu, Y. Zuo, S. Liu, Y. Dai, Analysis of
617 indoor VLC positioning system with multiple reflections, in: 2017 16th
618 International Conference on Optical Communications and Networks (IC-
619 OCN), 2017, pp. 1–3. doi:10.1109/ICOON.2017.8121297.
- 620 [32] J. O. Roa, A. R. Jiménez, F. Seco, J. C. Prieto, J. Ealo, Optimal
621 placement of sensors for trilateration: Regular lattices vs meta-heuristic
622 solutions, in: R. Moreno Díaz, F. Pichler, A. Quesada Arencibia (Eds.),
623 *Computer Aided Systems Theory – EUROCAST 2007*, Springer Berlin
624 Heidelberg, Berlin, Heidelberg, 2007, pp. 780–787.
- 625 [33] D. Plets, S. Bastiaens, L. Martens, W. Joseph, An analysis of the impact
626 of led tilt on visible light positioning accuracy, *Electronics* 8 (2019).
627 doi:10.3390/electronics8040389.

- 628 [34] E. Jeong, S. Yang, H. Kim, S. Han, Tilted receiver angle error compen-
629 sated indoor positioning system based on visible light communication,
630 *Electronics Letters* 49 (2013) 890–892. doi:10.1049/el.2013.1368.
- 631 [35] J. Kim, S. Yang, Y. Son, S. Han, High-resolution indoor positioning
632 using light emitting diode visible light and camera image sensor, *IET*
633 *Optoelectronics* 10 (2016) 184–192. doi:10.1049/iet-opt.2015.0073.
- 634 [36] B. Zhou, V. Lau, Q. Chen, Y. Cao, Simultaneous positioning and orien-
635 tating for visible light communications: Algorithm design and perfor-
636 mance analysis, *IEEE Transactions on Vehicular Technology* 67 (2018)
637 11790–11804. doi:10.1109/TVT.2018.2875044.
- 638 [37] Y. Almadani, M. Ijaz, S. Bastiaens, S. Rajbhandari, W. Joseph, D. Plets,
639 An experimental analysis of the effect of reflections on the performance
640 of visible light positioning systems in warehouses, in: *2019 IEEE 2nd*
641 *British and Irish Conference on Optics and Photonics (BICOP)*, 2019,
642 pp. 1–4.
- 643 [38] B. Neuwinger, U. Witkowski, U. Rückert, Ad-hoc communication
644 and localization system for mobile robots, in: *Advances in Robotics*,
645 Springer Berlin Heidelberg, Berlin, Heidelberg, 2009, pp. 220–229.
- 646 [39] K.-W. Lee, J.-B. Park, B.-H. Lee, Dynamic localization with hybrid
647 trilateration for mobile robots in intelligent space, *Intelligent Service*
648 *Robotics* 1 (2008) 221–235. doi:10.1007/s11370-007-0012-1.
- 649 [40] C. W. Chow, Y. Liu, C. H. Yeh, J. Y. Sung, Y. L. Liu, A practical
650 in-home illumination consideration to reduce data rate fluctuation in
651 visible light communication, *IEEE Wireless Communications* 22 (2015)
652 17–23. doi:10.1109/MWC.2015.7096280.